PCCP

PAPER

View Article Online
View Journal | View Issue

CrossMark click for updates

Cite this: *Phys. Chem. Chem. Phys.*, 2015, **17**, 23438

Electrochemical electron paramagnetic resonance utilizing loop gap resonators and micro-electrochemical cells†

Mika A. Tamski,[a] Julie V. Macpherson,[b] Patrick R. Unwin[b] and Mark E. Newton*[a]

A miniaturised electrochemical cell design for Electron Paramagnetic Resonance (EPR) studies is reported. The cell incorporates a Loop Gap Resonator (LGR) for EPR investigation of electrochemically generated radicals in aqueous (and other large dielectric loss) samples and achieves accurate potential control for electrochemistry by using micro-wires as working electrodes. The electrochemical behaviour of the cell is analysed with COMSOL finite element models and the EPR sensitivity compared to a commercial TE_{011} cavity resonator using 4-hydroxy-2,2,6,6-tetramethylpiperidin-1-oxyl (TEMPOL) as a reference. The electrochemical EPR performance is demonstrated using the reduction of methyl viologen as a redox probe in both water and acetonitrile. The data reported herein suggest that sub-micromolar concentrations of radical species can be detected in aqueous samples with accurate potential control, and that subtle solution processes coupled to electron transfer, such as comproportionation reactions, can be studied quantitatively using EPR.

Received 21st July 2015,
Accepted 12th August 2015

DOI: 10.1039/c5cp04259c

www.rsc.org/pccp

Open Access Article. Published on 13 August 2015. Downloaded on 2/14/2026 11:33:46 AM.
This article is licensed under a Creative Commons Attribution 3.0 Unported Licence.

Introduction

Electron Paramagnetic Resonance (EPR) is a spectroscopic technique that has been applied to electrochemical systems since the early work of Austen *et al.*[1] and Maki and Geske.[2] Due to its high sensitivity towards paramagnetic species, EPR can provide key information about radical species generated or consumed during electrode reactions. EPR thus complements electrochemical data by directly identifying radical species, confirming reaction mechanisms, and revealing more subtle interactions, for example, between the radical and its environment.[3,4] As such, EPR has not only provided a wealth of information to electrochemists, but EPR spectroscopists have also found electrochemical generation to be a feasible option to standard chemical and optical generation of radical species.[5,6]

There have been a number of approaches to the electrochemical (EC) cell design for EC-EPR, as evident from several reviews.[7–10] Due to significant dielectric losses at microwave frequencies, aqueous EC-EPR has typically involved the use of flat cells in conjunction with cavity resonators where the sample is as far as possible confined away from the electric fields in the resonator.[11–16] Electrochemical problems associated with these designs include significant ohmic-drop and large capacitive currents limiting the cell time constant.[17,18] Problems in terms of EPR performance can include the deterioration of the resonator Quality factor (Q-value) and hence EPR sensitivity due to the interaction of the microwave electric field with the metal electrodes and aqueous sample inside the resonator,[7] reproducible alignment of the electrochemical cell inside the resonator between experimental runs, and the inhomogeneity of the microwave magnetic field (B_1) inside a cavity resonator.[19] Flat cells may also be prone to convection during prolonged electrolysis times[6] leading to distortion of both the electrochemical and EPR performance.

Loop Gap Resonators (LGRs) were developed in the early 80's for EPR purposes[20] and were applied to EC-EPR by Allendoerfer *et al.*,[21] allowing aqueous samples to be investigated with 50 to 100 times larger absolute sensitivities compared to other resonator-EC cell combinations at the time. In a LGR, the microwave electric field is mostly confined in the gaps of the resonator, allowing aqueous or other dielectrically "lossy" samples to occupy a larger volume relative to the size of the resonator. In addition to favourable EPR performance in aqueous systems for very small sample volumes[22] (order of microliters), the smaller size of the resonator also allows the optimization of the electrochemical performance through miniaturization.

Ultramicroelectrode (UME) concepts have gone practically unnoticed in EC-EPR, although some examples of the use of small diameter wires exist.[23–25] Electrochemically, the benefits

[a] *Department of Physics, University of Warwick, Gibbet Hill Road, Coventry, CV4 7AL, UK. E-mail: m.e.newton@warwick.ac.uk*
[b] *Department of Chemistry, University of Warwick, Gibbet Hill Road, Coventry, CV4 7AL, UK*

† Electronic supplementary information (ESI) available: Fig. S1: The EC-EPR setup. See DOI: 10.1039/c5cp04259c

 This journal is © the Owner Societies 2015

Open Access Article. Published on 13 August 2015. Downloaded on 2/14/2026 11:33:46 AM.
This article is licensed under a Creative Commons Attribution 3.0 Unported Licence.

of UMEs include diminished ohmic drop, shorter cell time constants and enhanced mass transport.[26–28] However, for EC-EPR applications the small currents associated with UMEs can introduce significant challenges, as radical concentrations generated may be insufficient to allow the EPR study of short-lived intermediates or products. Among UMEs, the micro-cylindrical geometry is one of the simplest and easiest to fabricate and use and is particularly attractive in EC-EPR, as the length of the cylinder can be varied in order to produce the desired amount of current and thus generate a sufficient number of radicals *in situ*.[29–31]

Building on the early work of Allendoerfer *et al.*,[21] in this paper we report a new EC-EPR cell design that can be used with an X-band (8–12 GHz) LGR and water as a solvent. The use of micro-wire electrodes overcomes the electrochemical problems associated with flat cells, while the high sensitivity of the LGR makes the study of radical species possible, even with low currents. The design allows a range of working-, reference- and counter electrode (WE/RE/CE) materials and geometries to be used. Possible fouling of the WE can be addressed by exchanging the electrode without dissembling the entire cell and cell parts are reusable and interchangeable to allow maximum experimental flexibility.

Experimental

Cell design

A schematic of the cell designed for the EC-generation of radicals *in situ* within a LGR is shown in Fig. 1a. Parts 1, 3, 4 and 5 were machined from polyether ether ketone (PEEK) due to the mechanical and chemical stability of the material. Parts 1 and 3 support EPR test tubes, 2a: Q-band EPR tube 1.1 mm ID & 1.6 mm OD, 2b: X-band EPR tube 3.0 mm ID & 4.0 mm OD. 2a is the sample tube holding the solvent and therefore the ID determines the sample volume inside the resonator, but also contains the WE and RE. In an assembled set-up (Fig. 1b and Fig. S1, ESI†) the inner tube holds the solvent away from the fringing electric fields of the LGR gaps. Thus, if necessary, the ID of 2a can be adjusted by choosing a suitable capillary and the performance of the setup optimised for solvents with different dielectric constants. To date, cells with ID's (2a) between 0.8 and 1.1 mm have been fabricated. The X-band tube (2b) acts as a structural support, making the assembled cell robust and easy to handle, while enabling symmetrical placement of the cell into the resonator.

Screw threads (c) on part 3 allow the attachment of the cell into the resonator (Fig. 1b) and also the adjustment of the WE inside the resonator in the *Z*-direction for optimal performance. Part 4 fits to part 3, resulting in a small chamber between them where the CE is located. The four channels in part 4 allow the attachment of Teflon tubing for solvent flow, but also permit the connection of the RE and CE to thicker wires outside the cell for electrical connection through part 5. This arrangement makes changing the RE and CE easy if necessary, whilst the additional channel enables mixing experiments to be conducted.

Part 6 is a fine capillary with dimensions of *ca.* 0.15 mm ID, 0.4 mm OD through which the WE is guided to the sensitive part of the LGR inside 2a. The capillary can be removed and inserted back through part 4, allowing the WE to be changed when necessary. The bracketed part, from where the enlarged diagram is taken, represents the sensitive region of the 5-loop 4-gap LGR used in this work and has a length of 10 mm in the *Z*-direction. The RE, inserted into the cell through one of the pegs (5) is placed as close as possible to the WE to minimise the uncompensated resistance. The CE in the chamber of

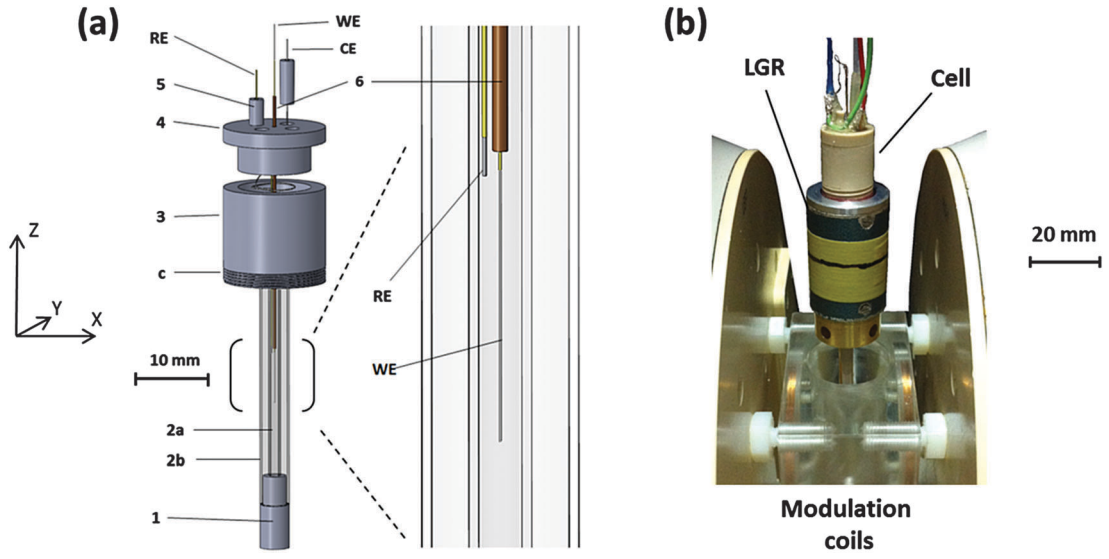

Fig. 1 (a) The EC-EPR cell designed for a LGR. 1 & 3: capillary supports, 3c: threads to attach the cell to the resonator, 2a: Q-band EPR tube for the sample, 2b: standard X-band EPR tube for structural support, 4: adaptor for electrodes and sample flow, 5: pegs for electrode attachment, 6: capillary for inserting the working electrode (WE) to the sensitive part of the resonator, RE: reference electrode, CE: counter electrode. (b) Image of the cell attached to the resonator. For experiments the resonator is lowered inside the modulation coils.

Open Access Article. Published on 13 August 2015. Downloaded on 2/14/2026 11:33:46 AM.
This article is licensed under a Creative Commons Attribution 3.0 Unported Licence.

parts 3 and 4 is far enough from the active region of the resonator so that no interference from CE products is expected.

Assembly

An image of the cell attached to the LGR is shown in Fig. 1b, and the LGR, in turn, is attached to a coupling arm. For experiments, the setup is lowered to the middle of the modulation coils, which are fastened between the EPR magnet poles. The in-house built modulation coils provide the high frequency modulation of the DC magnetic field necessary for the lock-in detection in continuous wave (CW) EPR experiments. The LGR attaches to the coupling arm and is coupled to the microwaves inductively[32,33] through a rigid coaxial cable with a coupling loop at the end. The coupling arm enables the distance between the resonator and the loop to be adjusted so that a critical coupling can be achieved for optimum sensitivity.

The sample is deoxygenated in a glass syringe by bubbling N_2 gas through it and introduced into the cell by a syringe pump (Legato 110) through PTFE tubing surrounded by a larger PVC tube. The interior of the PVC tubing is flushed with N_2 during the experiment and the flow guided through the whole of the central cavity of the modulation coils, thus creating an inert atmosphere around the entire EC-EPR setup, enabling high reproducibility for oxygen free experiments. Fig. S1 (ESI†) represents the setup in more detail.

Materials

Chemicals. Potassium chloride (BioXtra ≥99.0%), potassium nitrate (ReagentPlus®, ≥99.0%), paraquat dichloride (Methyl Viologen; PESTANAL®, analytical standard), tetrabutylammonium perchlorate (TBAP; Fluka, ≥99.0%), hexammine ruthenium(III) chloride (98%) and 4-hydroxy-TEMPO (TEMPOL; 97%) were purchased from Sigma-Aldrich. Milli-Q water (Millipore Corp.) (resistivity 18.2 MΩ cm, 25 °C) was used for aqueous work and anhydrous acetonitrile (Sigma, 99.8%) as an organic solvent. All chemicals were used as received. (Ferrocenylmethyl) trimethylammonium hexafluorophosphate ($FcTMA^+$) was prepared as described elsewhere.[34]

Electrode wires. WEs were 50 μm diameter Pt or Ag microwires coated with a 7.5 μm layer of polyester (Goodfellow, ±10% tolerance in conductor diameter). The desired length of polyester (typically 7 mm) was removed by soaking in saturated KOH. CEs were bare Pt or Ag wires, and either bare or chloridized Ag wires of diameter 50 μm or 125 μm served as REs. Before commencing EC or EC-EPR experiments, the WE was cycled in the appropriate background electrolyte within the potential range for the mediator of interest, until a stable response was recorded. The potential was controlled through a potentiostat (CH Instruments, CHI 1140B) in a three electrode configuration.

Simulations

The theory for the diffusion of electro-active species to a microcylindrical electrode has been developed for linear sweep experiments. Assuming uniformity along the cylinder, only a single dimension of diffusion has to be considered, and for a linear sweep the analytically obtained peak current density is:[29]

$$j_p = \frac{n^2F^2C^*av}{RT}\left(\frac{0.446}{p} + \frac{0.335}{p^{1.85}}\right) \quad (1)$$

where n is the number of electrons transferred in the redox process, F is the Faraday constant, C^* is the bulk concentration of the electroactive species, a is the radius of the cylinder, v the scan rate, R the universal gas constant and T the temperature in Kelvin. p is defined by:

$$p = \sqrt{nFa^2v/TRD} \quad (2)$$

where D is the diffusion coefficient of the electroactive species. For high scan rates or large wire diameters the values of p are also large, and the behaviour is dominated by linear diffusion, whereas for very slow scan rates or small electrode diameters p is small and the behaviour approaches the steady state-solution characteristic of micro electrodes.[31]

The WE placed inside a 0.8 mm ID sample tube (part 2a Fig. 1a) was modelled using COMSOL Multiphysics 4.4 (COMSOL AB) Finite Element Modelling (FEM) software. Fig. 2a shows a schematic representation of the model. The domain height and width are 11.2 and 0.4 mm respectively for the modelled 0.8 mm ID capillary in 2D axisymmetric geometry. Therefore, the model is not shown to scale, as the height of the domain is significantly greater than the width, but distinguishes the different types of boundaries used.

Boundary 1a is the wire electrode surface where the small edge (1b) represents the tip of the wire. Boundary 2a is the wire insulation with 2b representing the insulation edge (7.5 μm) at the electrode/insulation interface. Boundary 3 represents the bulk solution in the capillary far away from the WE. Boundary 4 is the capillary wall where the concentration of the electroactive

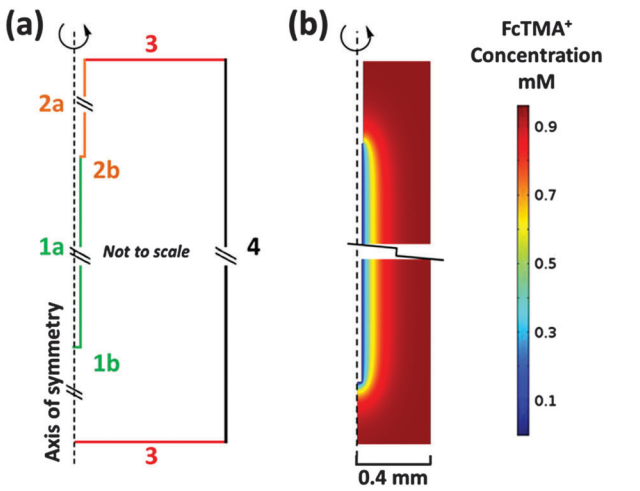

Fig. 2 2D axisymmetric COMSOL model. (a) Boundaries 1a & b: WE, 2a & b: insulation, 3: bulk concentration, 4: capillary wall. (b) A snapshot of the concentration of $FcTMA^+$ within the cell during a 20 mV s^{-1} cyclic voltammogram between 0 and 0.6 V at the switching potential for oxidation of 1 mM $FcTMA^+$ at a 50 μm diameter, 7 mm long, wire electrode.

Open Access Article. Published on 13 August 2015. Downloaded on 2/14/2026 11:33:46 AM.
This article is licensed under a Creative Commons Attribution 3.0 Unported Licence.

Table 1 Boundary conditions for the finite element model for CV. C^* = 1.0 mM $FcTMA^+$, T = 294 K, n = 1, E_0 = 0.356 V, E_{appl} swept between 0.0 and 0.6 V linearly over time, $C_{0,j}$ = [$FcTMA^+$] at the electrode surface as a function of the E_{appl}, F = 96 485 C mol^{-1} and R = 8.314 J mol^{-1} K^{-1}

Boundary	Boundary type	Boundary condition
1a 1b	Wire electrode Electrode tip	$\left\{\begin{array}{c} C_{0,j} = (C^*\theta)/(1+\theta) \\ \theta = \exp\left[\left(\frac{nF}{RT}\right)(E_0 - E_{appl})\right] \end{array}\right\}$
2a	Wire insulation	$n\cdot\nabla C = 0$
2b	Insulation edge	$n\cdot\nabla C = 0$
3	Bulk solution	$C = C^*$
4	Capillary wall	$n\cdot\nabla C = 0$
Axial symmetry		$n\cdot\nabla C = 0$

species goes to zero. Corresponding boundary conditions for the model are summarised in Table 1.

For 100 and 20 mV s^{-1} scan rates simulated, 20 000 and 15 000 mesh points were applied respectively along the 7 mm long wire electrode (boundary 1a) and 25 mesh points to the electrode tip (boundary 1b). The domain was then meshed continuously with a maximum element growth rate of 1.02 from the electrode surface.

$FcTMA^+$ oxidation and the subsequent reduction of $FcTMA^{2+}$ under diffusion control was modelled for cyclic voltammetry (CV) by solving Fick's second law for the concentration (C) of reactant species:

$$\frac{\partial C}{\partial t} = D_j \nabla^2 C \quad (3)$$

where t is time and ∇^2 is the Laplacian operator. The D of 6.7 × 10^{-6} cm^2 s^{-1} and the formal potential (E_0) of 0.356 V were determined using a 12.5 μm diameter disc UME in a bulk solution of 1 mM $FcTMA^+$ in 0.4 M KCl against a Ag|AgCl reference. Nernstian behaviour during CV was modelled at boundaries 1a & b, where the concentration of $FcTMA^+$ ($C_{0,j}$) relative to $FcTMA^{2+}$ was controlled by sweeping the applied potential (E_{appl}) between 0 and 0.6 V linearly over time.

Fig. 2b is a snapshot of the concentration of $FcTMA^+$ in the cell during a 20 mV s^{-1} CV recorded between 0 and 0.6 V at the switching potential of 0.6 V. The figure is zoomed to the electrode/insulation interface and to the wire tip and thus boundaries 3 where $C = C^*$ lie further away than suggested by the figure. A 0.8 mm ID sample tube (2a, Fig. 1a) was chosen for the model, as the simulations results were identical to those obtained with the wire electrode in a bulk solution, indicating that for a symmetrically placed WE, the cell wall does not hinder the diffusion field, and thus the model is representative of eqn (1) and (2).

The LGR

The role of the resonator is to concentrate the B_1 field in the sample and make the signal produced by the change in magnetic susceptibility at resonance as large as possible. Rather than trying to fit the experiment to general purpose cavity EPR resonators, LGR's provide the opportunity to adapt the resonator to the experiment. The CW EPR signal is proportional to the loaded resonator Q-value (Q_L) and the filling factor (η):[35]

$$S \propto Q_L \eta \quad (4)$$

For LGRs, Q_L (the ratio of the microwave energy stored in the resonator loaded with a sample to that dissipated per cycle when critically coupled to the microwave bridge) is, in general, lower than that for a traditional cavity resonator at the same frequency. Nonetheless, η (proportional to the ratio of ${B_1}^2$ integrated over the sample to ${B_1}^2$ integrated over the entire resonator) can be many times large than that for a high Q cavity, and the resulting ηQ_L product is often equal to or greater than that for a cavity. Also the more efficient separation of the microwave electric and B_1 fields in a LGR results in smaller dielectric losses when a lossy solvent is employed in the resonator.[36]

The use of LGR is particularly advantageous for samples of limited volume such as the concentration of short lived radical species in the diffusion field during an electrochemical experiment, and in cases where the sample is non-saturable and large B_1 fields can be used.[22] In addition, LGRs also allow the miniaturization of the electrochemical setup, enabling the beneficial use of microelectrodes.

EPR

A 5-loop 4-gap resonator was used for the EPR measurements. 4 gaps allow the increase in the diameter of the sample loop, thus facilitating the use of a standard 4 mm OD X-band EPR tube as a structural support. Bruker X-band continuous wave spectrometer (EMX-8/2.7) was used for the EPR measurements. Coupling to the microwave source (Bruker ER 041 X-band Microwave Bridge) was achieved using in-house built coupling arm and inductive coupling.

Results and discussion

The effect of the sample tube (2a) ID towards the EPR performance

The larger the ID of the sample tube, the closer the sample is to the fringing electric fields in the gaps of the LGR, leading to an increasing dielectric microwave loss. The unloaded Q-value (Q_u) of the 5-loop 4-gap resonator is approximately 1700 in accordance with the literature.[22] For water the 1.1 mm ID sample tube gives a typical Q_L = 500–600 at around 9.57 GHz, one third of the Q_u. If the cell is filled with acetonitrile, $Q_L \approx 900$. A cell assembled with the 0.8 mm ID sample tube filled with water gives a Q_L = 800–900 at around 9.51 GHz frequency. Crucially the insertion of a micro-cylinder WE to the resonator does not introduce a noticeable change in the Q-value or the microwave coupling.

Higher Q-values suggest higher sensitivity. However, eventually the diminishing ID of the capillary starts to hinder the electrochemical performance (see Fig. 4 and discussion) and a compromise between the two has to be made depending on the system under investigation.

Open Access Article. Published on 13 August 2015. Downloaded on 2/14/2026 11:33:46 AM.
This article is licensed under a Creative Commons Attribution 3.0 Unported Licence.

EPR sensitivity comparison between LGR and cylindrical resonator

The EPR performance between the LGR and a cylindrical TE_{011} resonator was compared by placing a 1.1 mm ID capillary filled with water containing 10 μM of the stable radical TEMPOL as a reference concentrically through each resonator. The TE_{011} cavity coupled critically with a Q-value of 1500, whereas the Q_u for this resonator was closer to 5000, suggesting that both resonators performed at approximately 1/3 of their Q_u. Using a microwave power sweep, saturation curves for both resonators were constructed. The optimal signal to noise ratio (S : N) achieved with both resonators was approximately 120 : 1 (Fig. 3), indicating that in terms of concentration sensitivity they perform equally. Note that the EPR spectrum for TE_{011} cavity is offset for clarity.

Although the two resonators performed similarly, taking into account sample volumes inside the resonators, in terms of absolute sensitivity the LGR performed 2–3 times better. In the future η for the LGR could be further increased by reducing the sample loop diameter leading to further sensitivity gains.

Electrochemistry

Experimental electrochemical characterization of two cells, representing the largest and smallest ID sample tubes used in this study, *i.e.* cell A (1.1 mm) and cell B (0.8 mm) are shown in Fig. 4a and b. The working electrode was a 50 μm diameter Pt wire, 7 mm in length, with 125 μm diameter Ag|AgCl RE and a bare Pt wire as a CE, while 0.4 M KCl acted as a supporting electrolyte. The results of the COMSOL simulation (identical for cells A and B) of the CV for the $FcTMA^{+/2+}$ are also shown in Fig. 4a and b.

Fig. 4a reveals that at scan rate of 100 mV s^{-1} the EC CV behaviour for the oxidation of 1 mM $FcTMA^{+}$ is very close to that predicted by the simulation assuming a reversible diffusion-controlled process. A peak to peak separation (ΔE_P) value of 78 mV is predicted from the simulation, which shows that diffusion is not purely linear at the micro-cylinder electrode. For cell A the simulated ΔE_P value is in good agreement with that recorded experimentally, *i.e.* 83 ± 2 mV. Note that increasing the supporting electrolyte concentration was observed to decrease the ΔE_P (due to Ohmic drop effects in the cell geometry employed) until values of *ca.* 0.4 M, beyond which increasing the concentration showed no appreciable effect. For the cell B measured ΔE_P value was 94 ± 2 mV, the difference to that obtained for cell A essentially due to a stretched out oxidative wave of the CV.

Fig. 4b shows the behaviour at 20 mV s^{-1} scan rate, where increased radial diffusion effects will contribute. This is reflected

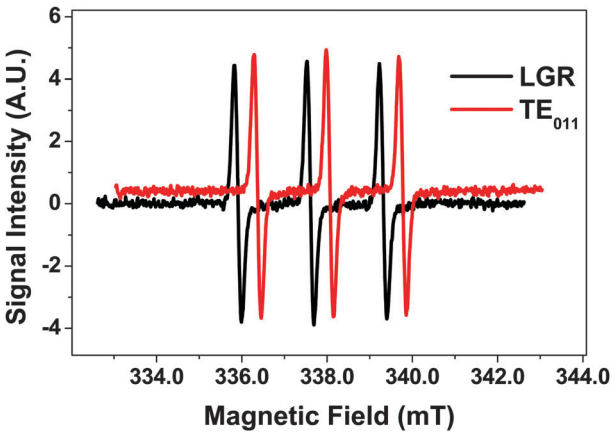

Fig. 3 1st derivative EPR spectra for 10 μM TEMPOL in LGR and TE_{011} with S : N = 120. Spectrum for TE_{011} is offset for clarity by 0.45 mT and 0.4 SI units.

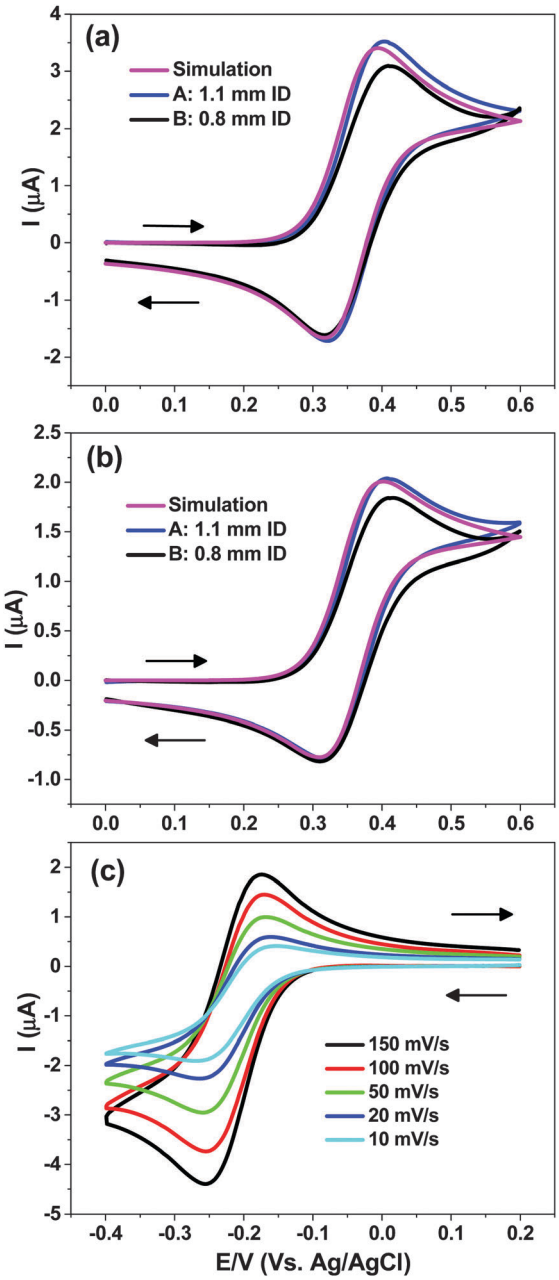

Fig. 4 Electrochemical characterization of cells A (1.1 mm ID) and B (0.8 mm ID) in water and comparisons with simulations. (a) 1.0 mM $FcTMA^{+}$; CV at 100 mV s^{-1}, (b) 1.0 mM $FcTMA^{+}$; CV at 20 mV s^{-1}, (c) 1.0 mM $Ru(NH_3)_6^{3+}$ at different scan rates. All results recorded at Pt wire electrode 50 μm in diameter, 7 mm length *vs.* Ag|AgCl reference and 0.4 M KCl as a supporting electrolyte.

This journal is © the Owner Societies 2015

Open Access Article. Published on 13 August 2015. Downloaded on 2/14/2026 11:33:46 AM.
This article is licensed under a Creative Commons Attribution 3.0 Unported Licence.

in a larger simulated ΔE_P = 93 mV which compares favourably with 94 ± 2 mV measured for cell A. For cell B the measured ΔE_P of 104 ± 2 mV suggests that at slower scan rates this cell behaviour is closer to that predicted.

For cell A, the experimental peak current (i_P) was within 3% of that simulated irrespective of the scan rate whereas for cell B the i_P value was consistently 8% lower. As discussed above in the simulations section, the capillary wall is not expected to hinder the diffusion field for 0.8 mm ID sample tube. A possible explanation for the slightly lower i_P and larger ΔE_P values is the fact that the WE is not completely symmetrically placed within the capillary. Thus the diffusion field might be restricted by the capillary wall, although the observed i_P values for cell B are still within the tolerance of the wire diameter (±10%) reported by the manufacturer.

The simulated i_P for the oxidation wave at 20 mV s^{-1} agreed with that predicted analytically (eqn (1) and (2)) to within 0.5%, and for 100 mV s^{-1} to within 2%. For the latter scan rate the no. of mesh points required to approach the value predicted by the analytical equations started to increase exponentially for an incremental increase in simulated i_P.

Fig. 4c shows reduction of $Ru(NH_3)_6^{3+/2+}$ for the cell A at different scan rates. The gradual change in the shape of the CV is evident as the measured ΔE_P increases from 80 to 114 mV as the scan rate is reduced from 150 to 10 mV s^{-1}. For mediators such as $Ru(NH_3)_6^{3+/2+}$ and $FcTMA^{+/2+}$, scan rates between 10 and 150 mV s^{-1} seem to be practical for the cell described.

Electrochemical EPR

EPR was carried out in the presence of the electrochemical redox mediator methyl viologen (MV^{2+}) which undergoes two consecutive one electron reduction steps, the first being:

$$MV^{2+} + e^- \leftrightharpoons MV^{+\bullet} \quad (5)$$

where the paramagnetic species $MV^{+\bullet}$ is formed. Previous work has shown this species to be sufficiently stable for convenient detection in EC-EPR.[16,37] A typical CV for the reduction of 1 mM MV^{2+} in water and 0.4 M KNO_3 at a Ag wire electrode (50 μm diameter, 7 mm length) for cell A is shown in Fig. 5a. The structure of the MV^{2+} is displayed in the inset to Fig. 5a. The ΔE_P value of 98 mV for a 20 mV s^{-1} scan rate suggests essentially a reversible behaviour, as discussed for Fig. 4b above and previously suggested by literature.[38,39]

From the CV in Fig. 5a a potential of −0.9 V was chosen to generate $MV^{+\bullet}$ under diffusion limited conditions. Fig. 5b shows the spectrum of the radical after electrolysing 1 mM MV^{2+} solution in the cell A for 2 min. The EPR scan was initiated as the potential was switched off.

The EPR spectrum obtained with 0.02 mT modulation, averaging 5 scans gave a signal to noise (S : N) of 740 : 1. The Root Mean Square (RMS) value for the noise was calculated from the baseline on a low field side of the spectrum. The emerging hyperfine coupling suggests that no line broadening occurs due to electron exchange between radical–parent interaction proposed previously:[24]

$$(MV^{+\bullet}) + (MV^{2+})^* \leftrightharpoons (MV^{+\bullet})^* + (MV^{2+}) \quad (6)$$

This is probably due to the relatively low concentration of the parent molecule with respect to the radical species in the active part of the resonator. In fact the best least squares fit yielded a line width of 0.017 mT for the smallest hyperfine couplings, further suggesting that the lines were not excessively broadened by radical–radical or radical–parent molecular interactions. Under these conditions the line width would exceed the used modulation amplitude of 0.02 mT. The result in 5b is in fact closer to those obtained for $MV^{+\bullet}$ productions through chemical reduction[40] or an exhaustive electrolysis of 1 mM MV^{2+} reported by Bard *et al.*[16]

A complementary option for scanning the magnetic field to record the entire EPR spectrum is to fix the field to a given value and monitor the signal amplitude as a potential perturbation is applied. This allows the generation of radical species at the electrode as a function of time and potential to be monitored simultaneously. Fig. 6 shows an average EPR signal amplitude

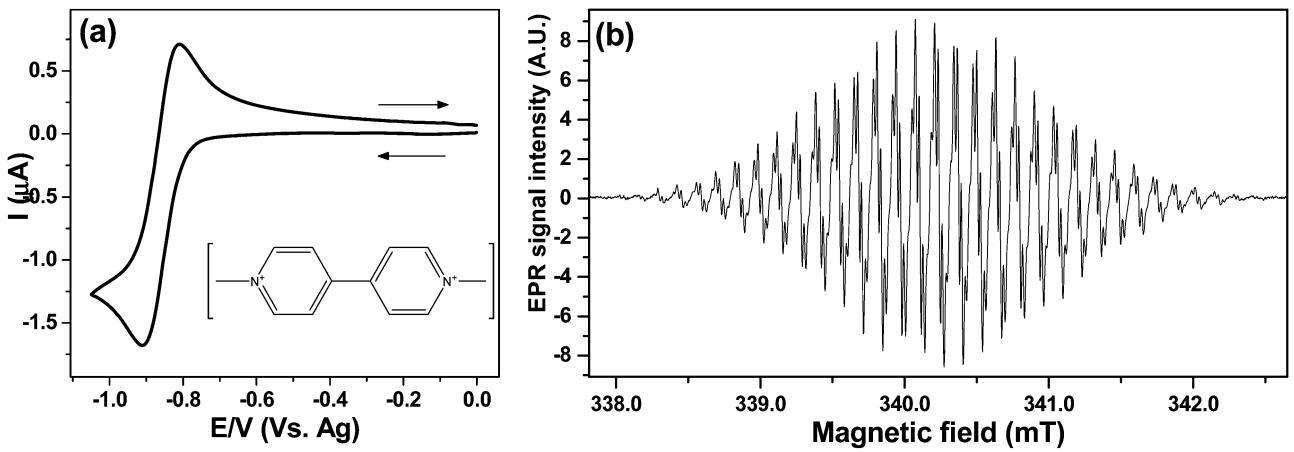

Fig. 5 EC-EPR in cell A: (a) CV at 20 mV s^{-1} for 1 mM MV^{2+} at a 50 μm Ag wire electrode *vs.* a Ag-pseudo reference in water with 0.4 M KNO_3, ΔE_P = 98 mV. Inset: The molecular structure of MV^{2+}. (b) EPR spectrum of $MV^{+\bullet}$ recorded after a 2 min potential step at −0.9 V, 2 mW microwave power, 0.02 mT modulation.

Open Access Article. Published on 13 August 2015. Downloaded on 2/14/2026 11:33:46 AM.
This article is licensed under a Creative Commons Attribution 3.0 Unported Licence.

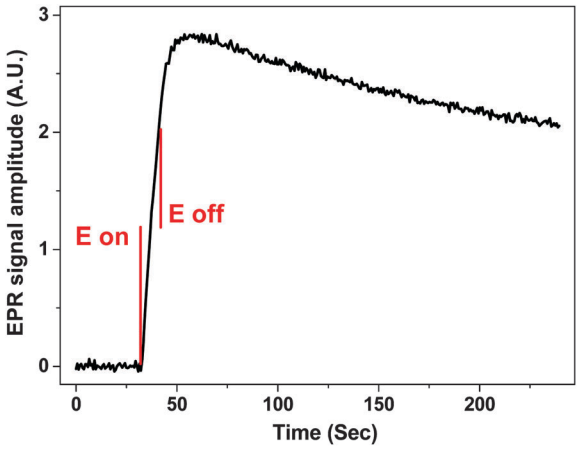

Fig. 6 5 scan average of the EPR signal amplitude at constant magnetic field as a function of potential and time during a 10 second potential step to −1.0 V from 0 V. 1 mM of MV^{2+} in water at 50 μM diameter Ag wire electrode *vs.* Ag pseudo RE and 0.4 M KNO_3 in the cell B. S : N = 122 : 1 with 2 mW microwave power and 0.1 mT modulation.

of 5 repetitions as a function of potential and time for 1 mM MV^{2+} in water and 0.4 M KNO_3, as the WE is stepped to −1.0 V for 10 seconds in cell B. Between the 5 repetitions, fresh solution was inserted to the cell *via* a syringe pump.

The charge generated during a 10 second potential step was *ca.* 1.4×10^{-5} C, indicating that the number of radical species ($MV^{+\bullet}$) generated was 8.7×10^{13}. The volume of sample inside the sensitive part of the resonator was 5 μL, and thus the concentration of the radical species can be estimated to *ca.* 30 μM, assuming 100% efficient electron transfer and that the radical decay is negligible during the relatively short potential step. The S : N = 122 : 1 when the signal was taken to be the maximum EPR amplitude, while for the noise a RMS was calculated from the region before the potential step. Extrapolating from the results in Fig. 6, the limit of quantification (LOQ) was estimated to be 7.1×10^{12} and the limit of detection (LOD) 2.1×10^{12} spins or 2.4 and 0.7 μM, respectively if the experiment was to be repeated 5 times.

The increase in the EPR signal shown in Fig. 6 is rapid after the potential step is applied at 32 seconds into the experiment. The EPR signal intensity increases for *ca.* 10 seconds after the potential switches off at 42 seconds, which could be attributed to the radical diffusing away from the electrode surface introducing changes to the filling factor and to the distribution of the radical within the B_1 field inside the sample volume. Also the formation of an EPR silent radical cation dimer in water has been proposed[41,42]

$$2MV^{+\bullet} \rightleftharpoons (MV)_2^{2+} \quad (7)$$

the presence of which could have an effect on the EPR signal at least on short timescales at the vicinity of the WE.

During the following 180 seconds after the potential was switched off the signal intensity decreased to 70% of the largest value, confirming the observation that $MV^{+\bullet}$ is indeed a stable radical in aqueous systems at least around neutral pH. No decay constant was calculated, as with the current setup it is possible that the stable radical could diffuse out of the sensitive part of the resonator within 180 seconds.

A wider potential sweep CV between −0.2 and −1.4 V for both reduction peaks of MV^{2+} is shown in Fig. 7a for cell B, corresponding to the electron transfer processes in eqn (5) and also eqn (8)

$$MV^{+\bullet} + e^- \rightleftharpoons MV^0 \quad (8)$$

where the paramagnetic one electron reduction product is further reduced to diamagnetic and EPR silent MV^0 species. An increase in the EPR signal amplitude (right *y*-axis) was observed (1) as the reduction in eqn (5) started to produce the paramagnetic species at the WE (left *y*-axis), and did not cease until the peak current for the second reduction step (2).

After this point, the EPR signal remained constant while the switching potential was reached and the scan reversed,

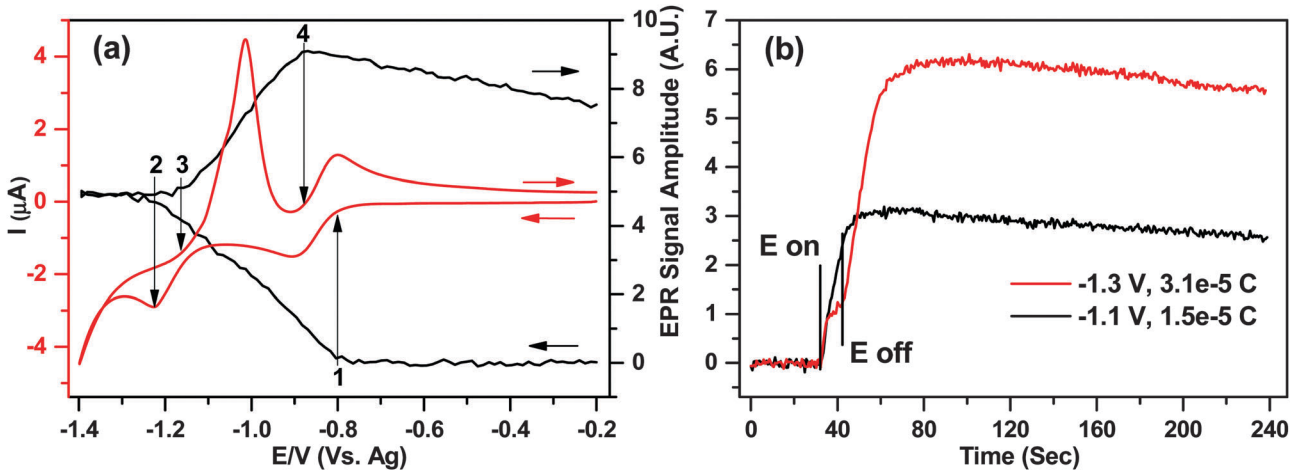

Fig. 7 (a) EPR signal amplitude (right *y*-axis) *vs.* redox processes for 1 mM $MV^{2+/1+\bullet/0}$ (left *y*-axis) in water during 20 mV s^{-1} CV; (b) EPR signal intensity *vs.* time during 10 second potential steps from −0.2 V to −1.1 V and −1.3 V. Both (a) and (b) with 50 μm diameter Ag wire electrode *vs.* Ag pseudo RE, 0.4 M KNO_3 in the cell B. 2 mW microwave power and 0.1 mT modulation.

Open Access Article. Published on 13 August 2015. Downloaded on 2/14/2026 11:33:46 AM.
This article is licensed under a Creative Commons Attribution 3.0 Unported Licence.

indicating that a steady concentration of radical species was maintained in the cell for *ca.* 20 seconds, at least on the EPR sensitivity scale. This result seems surprising as at high negative potentials the parent MV^{2+} molecule would be expected to reduce to MV^0, while the already generated $MV^{+\bullet}$ would also go through the second reduction step, thus leading to a diminishing EPR signal.

The EPR signal intensity started to increase again during the return scan at the onset of peak (3) on the voltammogram, where eqn (8) was reversed. The shape of the first oxidation peak during the reverse scan suggests a precipitation or deposition of the neutral MV^0 on the surface, and subsequent stripping from the electrode. This was also supported by the EPR as the rate of EPR signal increase between points (3) and (4) was *ca.* 25% larger than between (1) and (2), suggesting that the arrival of the species to the electrode surface exceeded the diffusion limit. Integration of the stripping peak yielded a charge of 2.5×10^{-5} C or 1.6×10^{14} molecules being oxidized during the reversal of eqn (8).

Finally the EPR signal intensity started to decrease at the onset of the second oxidation peak of the return wave (4) where eqn (5) was reversed. The signal intensity diminished by less than 20%, as the radical diffused throughout the sample volume and did not have time to arrive to the electrode for oxidation before the experiment finished.

The unexpected levelling of the EPR signal intensity at potentials beyond *ca.* −1.2 V in Fig. 7a was further investigated by applying two independent 10 second potential steps at −1.1 V and −1.3 V, corresponding to points just before and after the second reduction step, respectively. Fig. 7b displays the EPR amplitudes (*y*-axis) as a function of time (*x*-axis), and the applied potentials.

For the −1.1 V potential step corresponding to the process in eqn (5) the EPR signal increased as expected based on the data in Fig. 6 and *ca.* 1.5×10^{-5} C of charge was transferred. On the other hand, when the potential was stepped to −1.3 V, after the initial increase in the EPR signal a distinct plateau was observed, and the EPR signal increase didn't resume at the expected rate until the potential was switched off. None the less, as almost exactly twice the charge was generated during the step (3.1×10^{-5} C) combined with exactly double the EPR signal, there is a clear quantitative evidence that the final product in the solution is the paramagnetic $MV^{+\bullet}$ and not the neutral MV^0 that the applied potential would suggest.

From Fig. 7a it was determined that MV^0 is likely to deposit on the surface of the electrode, so the increase of the EPR signal after the potential is switched off at −1.3 V can be attributed to a process in eqn (9), proposed by Monk *et al.*[42]

$$MV^0 + MV^{2+} \rightarrow 2MV^{+\bullet} \quad (9)$$

although results reported therein did not display the quantitative behaviour described here. Due to an existing concentration gradient, MV^{2+} species still diffuses to the electrode surface after the potential step and can react with the MV^0 thus yielding two paramagnetic molecules. As long as there is an applied potential the paramagnetic product from eqn (9) is further reduced to the diamagnetic form and a plateau in the EPR signal intensity is observed.

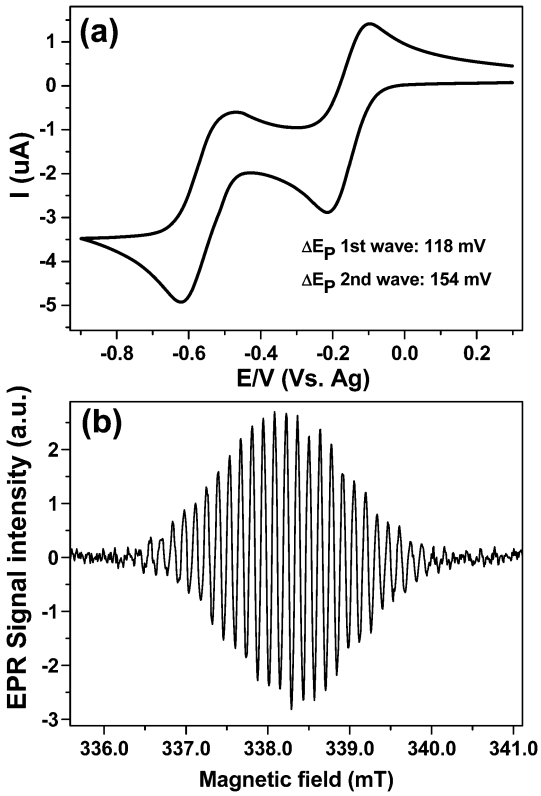

Fig. 8 1 mM MV^{2+}, 0.2 M TBAP in anhydrous acetonitrile at a 50 μm diameter Pt wire electrode *vs.* Ag-pseudo reference (a) 100 mV s^{-1} CV, (b) EPR spectrum of $MV^{+\bullet}$ in cell A, 2 mW microwave power, 0.05 mT modulation and 42 s scan time.

Clearly this setup allows the characterization of electrode processes under precise potential control on a quantitative level with high EPR sensitivity. In the future EC-EPR could be used for example to study comproportionation reactions, previously performed on UMEs, on equal or even lower redox mediator concentrations than before.[43]

Finally cell A was tested using a solvent with a moderate dielectric loss, acetonitrile. Fig. 8a displays the CV obtained at 100 mV s^{-1} scan rate over the both reduction steps for 1 mM MV^{2+} at a 50 μm diameter platinum WE *vs.* Ag-pseudo reference using 0.2 M TBAP as a supporting electrolyte. Clearly in acetonitrile the neutral MV^0 does not deposit on the electrode nor precipitate out of solution, at least to any significant extent, as both peaks of the return wave have a symmetry indicative of mass transport limitation, when compared to the CV in Fig. 7a. The larger cell resistance is obvious from the stretched ΔE_p value for the first wave (118 mV) when compared to the aqueous results.

The high EPR sensitivity is evident from Fig. 8b which was obtained after stepping the potential to −0.3 V with a single EPR scan for a concentration of *ca.* 20 μM of $MV^{+\bullet}$ giving S : N of 72 : 1 for 42 sec scan time, indicating that EC-ERP measurements are possible also with organic solvents.

Open Access Article. Published on 13 August 2015. Downloaded on 2/14/2026 11:33:46 AM.
This article is licensed under a Creative Commons Attribution 3.0 Unported Licence.

Conclusions

A novel design of EC-EPR cell has been presented and its electrochemical performance demonstrated with well-known redox mediators. The electrochemical EPR performance was analysed by characterising the behaviour of MV^{2+} in an aqueous system. These results suggest that the potential control of the cell is precise enough for analytical experiments, while the simultaneous EPR behaviour of the system can be monitored quantitatively under inert atmosphere.

Silver, gold and platinum can be used as a WE material between 25 and 125 μm conductor diameters. Also a piece of mesh has been inserted to the capillary instead of a wire and successful EC-EPR experiments performed, although at the expense of the potential control.

In terms of EPR sensitivity the LGR turned out to perform as well as commercially available cylindrical TE_{011} resonator. Sub μM EPR limits of detection have been demonstrated even for radicals such as $MV^{+\bullet}$ with complicated multi-line EPR spectra. Much lower detection limits are of course possible for radicals with simple single line EPR spectra. The sensitivity of the LGR allows the use of relatively small surface area micro wires and also a true miniaturization of the electrochemical cell. As the syringe pump/potentiostat/EPR interface can be programmed and thus certain experiments automated, signal averaging can be efficiently used to study short liver radicals.

Although designed primarily for aqueous samples, the applicability for organic solvents has also been demonstrated.

Obviously there are several parameters to optimise in EC-EPR, depending on the system under study. The design demonstrated here allows the maximum flexibility between the electrochemistry and EPR. Further work is underway for a detailed characterization of the setup for the routine absolute quantification of paramagnetic species in EC-EPR experiments.

Acknowledgements

The author would like to thank the EPSRC National EPR Research Facility & Service, Manchester for training in EC-EPR and the EPSRC Integrated Magnetic Resonance Centre for Doctoral Training (EP/J500045/1).

References

1 D. E. G. Austen, P. H. Given, D. J. E. Ingram and M. E. Peover, *Nature*, 1958, **182**, 1784–1786.
2 A. H. Maki and D. H. Geske, *J. Chem. Phys.*, 1959, **30**, 1356–1357.
3 A. J. Bard and L. R. Faulkner, *Electrochemical Methods: Fundamentals and Applications*, John Wiley & Sons, Inc., 2nd edn, 2001.
4 L. Dunsch, *J. Solid State Electrochem.*, 2011, **15**, 1631–1646.
5 P. H. Rieger, I. Bernal, W. H. Reinmuth and G. K. Fraenkel, *J. Am. Chem. Soc.*, 1963, **85**, 683–693.
6 L. H. Piette, P. Ludwig and R. N. Adams, *Anal. Chem.*, 1962, **34**, 916–921.
7 R. N. Bagchi, A. M. Bond and F. Scholz, *Electroanalysis*, 1989, **1**, 1–11.
8 A. M. Waller and R. G. Compton, in *Comprehensive Chemical Kinetics*, ed. R. G. Compton, Elsevier, 1989, vol. 29, pp. 297–352.
9 J. D. Wadhawan and R. G. Compton, in *Encyclopedia of Electrochemistry*, ed. A. J. Bard, M. Stratmann and E. J. Calvo, Wiley-VCH Verlag GmbH & Co. KGaA, 2003, vol. 29, pp. 170–220.
10 P. R. Murray and L. J. Yellowlees, *Spectroelectrochemistry*, The Royal Society of Chemistry, 2008, pp. 207–231.
11 B. A. Coles and R. G. Compton, *J. Electroanal. Chem.*, 1983, **144**, 87–98.
12 R. G. Compton, P. J. Daly, P. R. Unwin and A. M. Waller, *J. Electroanal. Chem.*, 1985, **191**, 15–29.
13 H. Park, M. S. Won, C. Cheong and Y. B. Shim, *Electroanalysis*, 2002, **14**, 1501–1507.
14 A. Petr, L. Dunsch and A. Neudeck, *J. Electroanal. Chem.*, 1996, **412**, 153–158.
15 E. Dmitrieva, Y. Harima and L. Dunsch, *J. Phys. Chem. B*, 2009, **113**, 16131–16141.
16 J. G. Gaudiello, P. K. Ghosh and A. J. Bard, *J. Am. Chem. Soc.*, 1985, **107**, 3027–3032.
17 I. B. Goldberg, A. J. Bard and S. W. Feldberg, *J. Phys. Chem.*, 1972, **76**, 2550–2559.
18 I. B. Goldberg and T. M. McKinney, in *Laboratory techniques in electroanalytical chemistry*, ed. P. T. Kissinger and W. R. Heineman, Dekker, New York, 1984, pp. 675–728.
19 R. N. Adams, *J. Electroanal. Chem.*, 1964, **8**, 151–162.
20 W. Froncisz and J. S. Hyde, *J. Magn. Reson.*, 1982, **47**, 515–521.
21 R. D. Allendoerfer, W. Froncisz, C. C. Felix and J. S. Hyde, *J. Magn. Reson.*, 1988, **76**, 100–105.
22 J. S. Hyde and W. Froncisz, in *Advanced EPR: applications in biology and biochemistry*, ed. A. J. Hoff, Elsevier, 1989, pp. 1–29.
23 R. N. Bagchi, A. M. Bond and R. Colton, *J. Electroanal. Chem.*, 1986, **199**, 297–309.
24 R. N. Bagchi, A. M. Bond and F. Scholz, *J. Electroanal. Chem.*, 1988, **252**, 259–267.
25 D. A. Fiedler, M. Koppenol and A. M. Bond, *J. Electrochem. Soc.*, 1995, **142**, 862–867.
26 M. Fleischmann and S. Pons, *J. Electroanal. Chem.*, 1987, **222**, 107–115.
27 S. Pons and M. Fleischmann, *Anal. Chem.*, 1987, **59**, A1391–A1399.
28 J. Heinze, *Angew. Chem., Int. Ed. Engl.*, 1993, **32**, 1268–1288.
29 K. Aoki, K. Honda, K. Tokuda and H. Matsuda, *J. Electroanal. Chem.*, 1985, **182**, 267–279.
30 K. Aoki, K. Honda, K. Tokuda and H. Matsuda, *J. Electroanal. Chem.*, 1985, **186**, 79–86.
31 K. Aoki, *Electroanalysis*, 1993, **5**, 627–639.
32 M. Mehdizadeh, T. K. Ishii, J. S. Hyde and W. Froncisz, *IEEE Trans. Microwave Theory Tech.*, 1983, **31**, 1059–1064.
33 G. A. Rinard, R. W. Quine, S. S. Eaton and G. R. Eaton, *J. Magn. Reson., Ser. A*, 1993, **105**, 137–144.
34 I. Dumitrescu, P. R. Unwin and J. V. Macpherson, *Electrochem. Commun.*, 2009, **11**, 2081–2084.

35 M. Brustolon, *Electron Paramagnetic Resonance, A practitioner's Toolkit*, A John Wiley & Sons, Inc., Hoboken, New Jersey, 2009.
36 G. Rinard and G. Eaton, in *Biomedical EPR, Part B: Methodology, Instrumentation, and Dynamics*, ed. S. Eaton, G. Eaton and L. Berliner, Springer US, 2005, vol. 24/B, pp. 19–52.
37 L. Zhuang and J. Lu, *Rev. Sci. Instrum.*, 2000, **71**, 4242–4248.
38 R. M. Elofson and R. L. Edsberg, *Can. J. Chem.*, 1957, **35**, 646–650.
39 C. L. Bird and A. T. Kuhn, *Chem. Soc. Rev.*, 1981, **10**, 49–82.
40 W. R. Dunham, J. A. Fee, L. J. Harding and H. J. Grande, *J. Magn. Reson.*, 1980, **40**, 351–359.
41 E. M. Kosower and J. L. Cotter, *J. Am. Chem. Soc.*, 1964, **86**, 5524–5527.
42 P. M. S. Monk, R. D. Fairweather, M. D. Ingram and J. A. Duffy, *J. Chem. Soc., Perkin Trans. 2*, 1992, 2039–2041.
43 C. Amatore, M. F. Bento and M. I. Montenegro, *Anal. Chem.*, 1995, **67**, 2800–2811.

Open Access Article. Published on 13 August 2015. Downloaded on 2/14/2026 11:33:46 AM.
This article is licensed under a Creative Commons Attribution 3.0 Unported Licence.